buildings

MDPI

Article

Study on the Static Characteristics of Lignin-Fiber-Reinforced Sand

Haihua Yang [1,2,3,*], Yongde Ai [1,2], Youjian Song [1], Ke Yang [1,2], Chaohong Chen [3,4] and Guanping Zou [1,2]

1 College of Hydraulic and Civil Engineering, Xinjiang Agricultural University, No. 311 Nongda East Road, Shaibak District, Urumqi 830052, China
2 Technical Research Center of Xinjiang Hydro-Geotechnical and Structural Engineering, Urumqi 830052, China
3 Key Laboratory of Dam Construction Safety and Disaster Prevention of Xinjiang Production and Construction Corps, Urumqi 830052, China
4 XPCC Surveying & Designing Institute Group Co., Ltd., Urumqi 830002, China
* Correspondence: yanghaihua@xjau.edu.cn

Abstract

In this study, compression, rebound, and triaxial tests were conducted to investigate the strength and deformation behavior of lignin-fiber-reinforced sandy soil under various conditions, with a focus on the influence of fiber content (FC) on its mechanical properties. Based on the experimental results, a modified Duncan–Chang model suitable for lignin-fiber-reinforced sandy soil was established. The results indicate that the addition of lignin fibers increases the compressive deformation of sandy soil. Under saturated conditions, the fibers suppress compressive deformation while enhancing rebound deformation, with the minimum compressive deformation observed at an FC of 0.5%. Quantitative analysis shows that as FC increases, the effect of dry and saturated states on compression and rebound indicators gradually diminishes. When the FC reaches 5%, these indicators are no longer significantly affected by moisture conditions. The inclusion of fibers also improves the shear strength of sandy soil. With increasing FC and confining pressure, the stress–strain curves gradually transition to a strain-hardening type. At an FC of 5% and under confining pressures of 100 kPa and 200 kPa, the stress–strain curves exhibit a more pronounced hardening trend compared to those at other fiber contents; under a confining pressure of 300 kPa, the curve exhibits a strain-hardening type. As FC increases, the specimens initially show dilatancy followed by contraction. The curves calculated using the modified Duncan–Chang model are in good agreement with the experimental data, validating the model's feasibility in capturing softening-type stress–strain behavior.

Keywords: lignin-fiber-reinforced sandy soil; compression index; shear strength; strain softening; Duncan-Chang modified model

Check for updates

Academic Editors: Meen-Wah Gui, Thang Pham and Phan Truc T.T.

Received: 2 March 2026
Revised: 5 April 2026
Accepted: 9 April 2026
Published: 14 April 2026

1. Introduction

Sandy soils are a type of specialized soil widely distributed around the world. Acting as a porous medium, they exhibit brittle mechanical behavior under external loads, which varies with environmental conditions [1,2]. In engineering construction, the strength characteristics of soils are often required to meet high standards to ensure long-term project stability. Therefore, there is an urgent need to develop various soil reinforcement techniques to enhance the mechanical properties of soils in geotechnical engineering [3,4]. Currently, soil reinforcement technologies have been implemented in more than a dozen countries and regions worldwide, and the reinforcement material systems involved span a diverse spectrum, ranging from traditional compounds to high-performance polymers [5]. Geosynthetic products are favored for their processing flexibility, high performance, and low cost [6]. The concept and principles of fiber reinforcement for soils were first proposed by Vidal in 1969, who found that incorporating fibers into soils can effectively improve their shear properties [7,8]. These materials act as geosynthetic reinforcement media, enhancing the mechanical properties and stability of soils through fiber reinforcement mechanisms [4,9]. Traditional synthetic fiber materials are mainly derived from petroleum by-products. As petroleum is a finite, non-renewable resource, this dependence poses challenges in terms of sustainability [10]. In recent years, natural fiber–soil composite reinforcement technology has rapidly emerged as a green soil improvement technique, offering broad application prospects in geotechnical engineering due to its environmental friendliness and cost-effectiveness [11–13]. Compared with traditional synthetic fibers, natural fibers can significantly reduce energy consumption and production costs [14]. The use of natural fibers as soil reinforcement materials aligns with sustainability requirements, demonstrating great potential and attracting increasing attention in the field of geotechnical engineering.

The Duncan–Chang model is favored for its simple form, few parameters, and ease of solution, and has been widely used in studies of soil constitutive models [15,16]. To better describe the stress–strain behavior of improved soils, numerous scholars have introduced modifications. He et al. used lime to improve dispersive soils and modified the Duncan–Chang model to account for lime curing age; the modified model accurately predicted the stress–strain curves of soils aged beyond 28 days [17]. Yang et al. reinforced red clay with coconut fibers and adapted the Duncan–Chang model, achieving a good fit for the stress–strain relationship of the fiber-reinforced soil [18]. Zhao et al. used polypropylene fibers to reinforce sandy soil and found that the Duncan–Chang model could describe the stress–strain behavior of this fiber-reinforced soil; they also proposed a method for determining the model parameters, providing a reference for accurately characterizing the mechanical properties of heavy railway subgrades [16]. Although progress has been made in the study of natural fiber-reinforced soils, a significant research gap remains regarding the use of lignin fiber to reinforce poorly graded fine sand. Lignin fiber, a solid waste resource derived from the paper industry, exhibits unique characteristics such as slight expansion upon water absorption, a porous surface, and high compressibility. Its interaction mechanism with poorly graded fine sand—including the synergistic effects of pore filling, particle bonding, and self-deformation—remains unclear. Existing studies have not revealed the quantitative effects of fiber content on the compression, rebound, and shear strength of sand, nor have they clarified the coupling mechanisms among dry/saturated states, confining pressure, and fiber content. Current Duncan–Chang modified models are primarily designed for synthetic fibers, other natural fibers, or modified clay systems, and are not suitable for the dynamic mechanical behavior of lignin fiber-reinforced sand, which exhibits strain softening under low confining pressure and strain hardening under high confining pressure. Moreover, these models lack systematic descriptions of the fitting process and parameter determination methodologies, making it difficult to provide a highly accurate and operable constitutive tool for this novel reinforcement system.

https://doi.org/10.3390/buildings16081532

At the engineering application level, there is an urgent need to reinforce poorly graded fine sand foundations, which are widely distributed in water conservancy projects in western China. However, the optimal fiber content range and quantitative evaluation standards for the reinforcement effect have not yet been established. Existing research has not formed engineering technical references that can be directly implemented, hindering the promotion and application of this environmentally friendly and efficient reinforcement technology.

Given the current state of application of natural fibers in sandy soils, it remains a relatively new technology. Moreover, existing studies on the modification of the Duncan-Chang model have mostly focused on systems such as lime-improved soil, coconut fiber-reinforced lateritic clay, and polypropylene fiber-reinforced sandy soil. Further research is therefore needed [16–19]. The research status of fiber-reinforced soil and constitutive modeling is shown in Table 1 [20–34]. This study aims to investigate the shear strength behavior of sand under different lignin fiber contents (FC) through laboratory compression–rebound tests and consolidated–drained triaxial compression tests. Based on the experimental data, the stress–strain relationship of the reinforced sand is analyzed to reveal its behavior under varying fiber contents and confining pressures. Building upon the Duncan–Chang model, key parameters—namely the peak deviatoric stress, its corresponding strain, and the initial elastic modulus—are introduced as core modification parameters. A modified Duncan–Chang model is then developed to accurately capture the strain-softening characteristics of lignin fiber-reinforced sand and to represent its dynamic softening–hardening transition behavior. This approach addresses the limitations of earlier Duncan–Chang models for fiber-reinforced soils and provides technical support for relevant engineering applications.

Table 1. Research status of fiber-reinforced soil and constitutive modeling.

Reference	Research Content	Research Methods	Core Contributions	Main Limitations
Diambra et al., 2013 [21]	A macro-scale constitutive model for fiber-reinforced sand	Volumetric averaging approach based on triaxial test results, superimposing contributions of sand and fibers	Developed a constitutive model accounting for fiber content, orientation, slip/pull-out, and effects on sand relative density.	Complex model with many parameters, limiting engineering applicability; validation limited to triaxial compression and extension.
Soltani et al., 2018 [26]	Swell-compression characteristics of fiber-reinforced expansive soil	Oedometer swell-compression tests with varying fiber type, content, and aspect ratio	Found that tape-shaped fibers effectively mitigate swelling and shrinkage; fiber content has greater effect than aspect ratio; wider fibers are more efficient; proposed a hyperbolic model to simulate swell-compression behavior.	Did not investigate wetting-drying cycles on long-term performance; model parameters are specific to the fibers and soil used.
Peng et al., 2019 [15]	Influence of freeze–thaw cycles on mechanical properties and Duncan-Chang model parameters of saline soil	Unconsolidated undrained triaxial tests on remolded samples with different salt contents and freeze–thaw cycles	Established a modified Duncan-Chang model considering freeze–thaw cycles; provided regression formulas for model parameters.	Model does not account for effect of freeze–thaw cycles on Poisson's ratio; tests were on remolded soil, which may differ from undisturbed soil.

Table 1. *Cont.*

Reference	Research Content	Research Methods	Core Contributions	Main Limitations
Abbaspour & Narani et al., 2020 [20]	Static and dynamic behavior of sandy subgrade reinforced with waste tire textile fibers	High-cycle cyclic loading triaxial tests with varying fiber contents	Investigated permanent strain, resilient modulus, energy dissipation, and damping ratio of WTTF-reinforced soil; classified materials based on shakedown theory (0–2% plastic shakedown, 3–4% plastic creep); resilient modulus increased by 744% at 2% fiber content; proposed prediction models for permanent strain and resilient modulus.	Tests used only one loading waveform and stress level; cyclic degradation of fiber–soil interface not thoroughly investigated; reinforcement effect weakens when fiber content exceeds 2%.
Jia et al., 2020 [28]	Modified Duncan-Chang model for modeling supported excavations in granular soils	Consolidated drained triaxial tests with varying relative density and confining pressure; proposed a novel disturbance function based on disturbed state concept	Modified the Duncan-Chang model to account for relative density effects on parameters K and M; outperformed Mohr-Coulomb model in numerical simulations of excavation problems.	Validation limited to a specific sand; disturbance function is empirical and requires further verification.
Yi & Du, 2020 [27]	Shear properties of geosynthetic-reinforced tailings	Triaxial compression tests with varying reinforcement layers (geogrid/geotextile)	Revealed that the number of reinforcement layers affects stress–strain curve shape (hardening/softening); proposed that "pseudo-cohesion" increases linearly with the number of reinforcement layers.	Did not consider evolution of interface characteristics between reinforcement and tailings during loading; tests were undrained, which may not reflect all field conditions.
Zhao et al., 2020 [16]	Polypropylene fiber-reinforced sand	Triaxial test, Duncan-Chang model	Proposed a method for determining model parameters.	Used synthetic fibers, natural fibers were not considered.
Kumar et al., 2021 [29]	Static and dynamic characterization of fiber-reinforced sand using numerical simulation	FLAC^{3}D numerical simulations with randomly distributed fiber elements	Successfully obtained elastic modulus, shear modulus, and damping ratio through numerical simulation of static and dynamic triaxial tests; analyzed the effect of fiber content.	Fiber-soil interface parameters were based on simplified assumptions without experimental calibration; fiber bending and torsion were not considered.
Salih et al., 2021 [23]	Mechanical properties of soil bricks reinforced with chicken feather and sugarcane bagasse fibers	Compressive and flexural strength tests on cubic and prismatic specimens at different fiber contents and curing ages	Determined optimal fiber content (7% for CFF, 5% for SBF) and length (15 mm); established a stress–strain constitutive model.	Fibers are susceptible to long-term degradation, affecting brick durability; proposed model has limited applicability period.

https://doi.org/10.3390/buildings16081532

Table 1. *Cont.*

Reference	Research Content	Research Methods	Core Contributions	Main Limitations
Shen et al., 2021 [32]	Strength characteristics of fiber-reinforced clayey soil treated with lime or cement	Consolidated undrained triaxial and unconfined compressive strength tests on untreated, lime-treated, and cement-treated soil with varying fiber content	Revealed the combined reinforcement effect of fibers and lime/cement; demonstrated that fibers can improve the brittle failure mode of lime/cement-treated soil.	Limited to one fiber type (polyester) and specific stabilizer contents; micro-mechanisms were not analyzed in depth.
Zhao et al., 2021 [25]	Dynamic behavior of natural and fiber-reinforced soils in heavy-haul railway embankments	Dynamic triaxial tests with varying water content, compaction degree, fiber content, length, and confining pressure	Developed empirical formulas for predicting maximum dynamic shear modulus, ultimate shear stress, and damping ratio.	Empirical formulas have limited applicability; evolution of fiber-soil interface under cyclic loading was not thoroughly studied.
Moslemi et al., 2022 [34]	Lignocellulosic fiber-reinforced sandy soil	Consolidated undrained triaxial tests with microstructural analyses, varying fiber type, content, length, and curing time	Found that fibers with higher pure cellulose content provide better reinforcement; revealed that reinforcement primarily enhances effective cohesion through physical mechanisms (interfacial friction).	Fibers are susceptible to biodegradation, affecting long-term performance; durability was not evaluated.
Lu et al., 2022 [33]	Mechanical and hydraulic behavior of fiber-reinforced cemented soil with fly ash	Consolidated undrained triaxial and permeability tests on composites with different binder combinations (cement, fly ash, sisal fiber)	Systematically compared the mechanical and hydraulic properties of four composite materials; found that the combination of fly ash and sisal fiber significantly increased peak strength.	Limited to one soil and fiber type; long-term fiber durability and environmental impacts were not considered.
Tang et al., 2022 [30]	Duncan-Chang model considering thixotropy of Zhanjiang Formation clay	Consolidated drained triaxial tests with varying resting times	Established quantitative relationships between curing time and strength parameters (cohesion, friction angle) as well as initial tangent modulus; integrated these into the Duncan-Chang model to propose a thixotropic constitutive model.	Model involves numerous parameters, making calibration complex; explanation of thixotropic mechanism is primarily macroscopic.
Kannan & Sujatha, 2023 [31]	Nano-silica and banana fiber-reinforced organic silt	Unconfined compressive strength and hydraulic conductivity tests	Demonstrated that nano-silica enhances the strength of fiber-reinforced soil, while fibers mitigate the brittle failure induced by nano-silica; revealed the composite reinforcement mechanism.	Triaxial tests were not conducted; dispersion and uniformity of nano-silica are difficult to control, affecting result stability.

Table 1. *Cont.*

Reference	Research Content	Research Methods	Core Contributions	Main Limitations
Yang et al., 2023 [18]	Coir fiber-reinforced laterite	Triaxial test, Modified Duncan-Chang model	Improved the fitting accuracy of the stress–strain relationship of laterite.	Focused on clay and is not applicable to poorly graded fine sand.
Zafar et al., 2024 [22]	A review of soil stabilization using natural and synthetic fibers	Literature review	Systematically reviewed the effects of various natural and synthetic fibers on the mechanical properties (CBR, UCS, etc.) of expansive soils and fly ash-stabilized soils.	Review paper without new experimental data; discussion on reinforcement mechanisms and long-term performance is not in-depth.
He et al., 2024 [17]	Lime-modified dispersive soil	Triaxial test, Age-modified model	Enables prediction of the long-term mechanical properties of soil.	Chemical stabilization was adopted, without addressing the reinforcement mechanism of natural fibers.
Shu et al., 2024 [24]	MICP synergistic fiber reinforcement for sand stabilization	Literature review	Systematically summarized the mechanisms of eight fiber types in MICP-treated sand; pointed out that the two-step injection method improves calcium carbonate distribution uniformity; fiber content has a greater effect on UCS than fiber length; fiber type has a greater effect than fiber length.	Review paper without new experimental data; did not cover all fiber types; limited analysis of practical applications.
Song et al., 2025 [35]	Dynamic characteristics of lignin fiber-reinforced sand	Dynamic triaxial test	Revealed the evolution patterns of dynamic elastic modulus and damping ratio.	Only dynamic characteristics were investigated, while compression, rebound, and static constitutive behavior were not examined.
This study	Static characteristics of lignin fiber-reinforced poorly graded fine sand	Triaxial test, Compression-rebound test, Duncan-Chang model	Revealing the coupled effects of dry/saturated state, fiber content, and confining pressure; Proposing a modified model adapted to the softening-hardening transition	-

2. Overview of the Test

2.1. Test Equipment and Materials

The test equipment used in this study includes the WG-type single-lever consolidometer (Nanjing Soil Instrument Factory Co., Ltd., which is located in Nanjing, China) and the small dynamic and static triaxial (Tianshui Hongshan Testing Machine Co., Ltd., and this manufacturer is located in Xinjiang, China) testing system from the Technical Research Center of Xinjiang Hydro-Geotechnical and Structural Engineering. The WG-type single-lever consolidometer is used to determine the consolidation and rebound characteristics of soil under one-dimensional compression, including the compression coefficient, compression modulus, compression index, and rebound index. It is a standard testing device for evaluating foundation settlement and soil deformation behavior.

The triaxial testing system accommodates both static and dynamic tests on specimens with diameters of 39.1 mm and 80 mm. The axial force and confining pressure are applied using a hydraulic servo actuator, which enables cyclic loading tests under various dynamic stresses in the axial direction. The dynamic loading frequency ranges from 0.01 to 5.00 Hz, the maximum axial force is 25 kN, and the maximum confining pressure in the pressure chamber is 1 MPa. The test apparatus is shown in Figure 1.

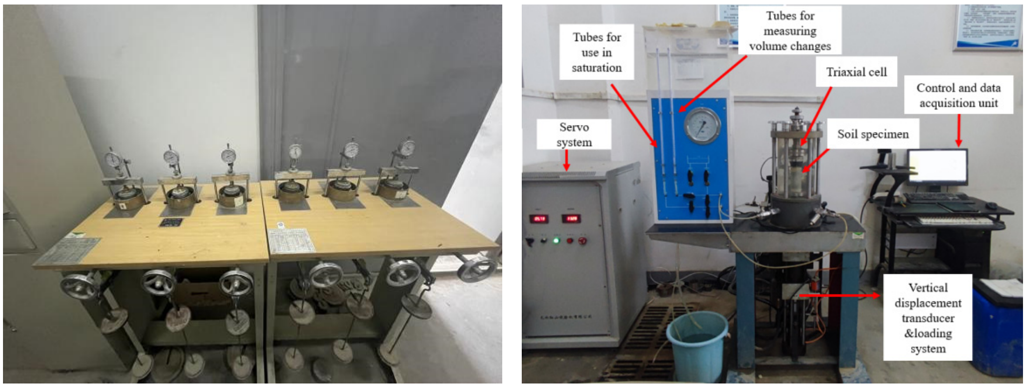

(**a**) Model WG Single Lever Consolidator (**b**) Triaxial Test Apparatus

Figure 1. Experimental equipment.

The soil sample used in this test was collected from the foundation sand of a water conservancy project in southern Xinjiang. According to ASTM D2487-17, *Standard Practice for Classification of Soils for Engineering Purposes (Unified Soil Classification System)* [36], the sand has a fines content (particle size < 0.075 mm) of less than 5%, with a uniformity coefficient $C_u = 4.46$ and a curvature coefficient $C_c = 2.35$. Although C_c falls within the reasonable range of 1–3, the condition $C_u < 6$ classifies the sand as poorly graded fine sand (SP). Its particle size distribution curve is shown in Figure 2, and its physical and mechanical property indices are presented in Table 2.

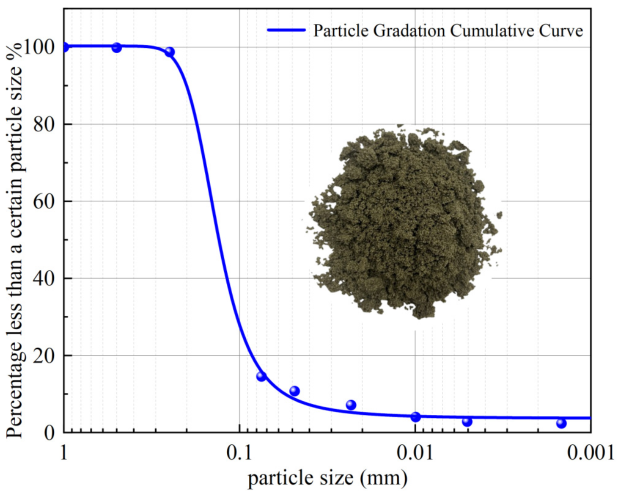

Figure 2. Grain size distribution curve of test sand and soil.

Table 2. Basic physical indicators of sandy soil.

Average Particle Size D_{50}/mm	Coefficient of Inhomogeneity C_u	Curvature Factor C_c	Specific Gravity of Soil G_s	Maximum Dry Density ρ_{dmax} (g/cm^3)	Minimum Dry Density ρ_{dmin} (g/cm^3)	Relative Density D_r
0.124	4.46	2.35	2.69	1.78	1.32	0.8

The reinforcement material used in this study is lignin fiber, a natural plant-based fiber prepared by the fibrillating modification of poplar alkali lignin extracted from industrial alkali-method papermaking black liquor. As a product of solid waste resource utilization in the paper industry, it offers both environmental benefits and the advantage of local raw material availability. The fiber appears as a light-yellow powder, with an irregular network-like interwoven structure at the microscopic level. Its surface is rough and contains numerous micropores and grooves, as shown in Figure 3.

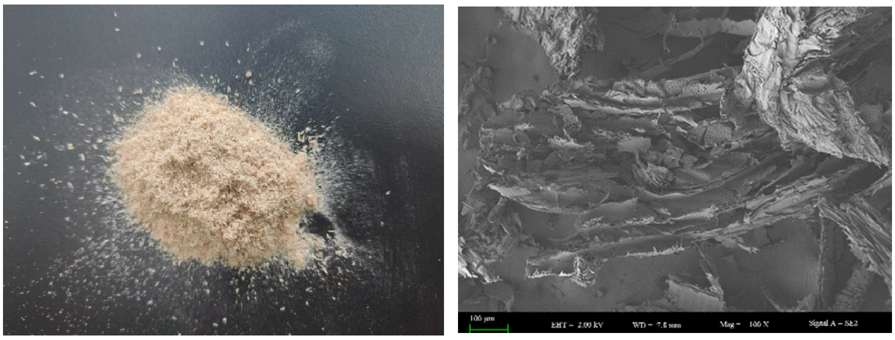

(**a**) Macroscopic morphology (**b**) Microscopic morphology

Figure 3. Lignin fiber macro- and micro-morphology.

The primary chemical component of the fiber is lignin ($\geq$85%), accompanied by 3–5% cellulose, 2–4% hemicellulose, and $\leq$1% inorganic ash. The lignin molecule contains a large number of polar functional groups, such as hydroxyl and methoxy groups, which form the basis for the fiber's adhesion and water absorption properties. Laboratory tests indicate that the fiber has a saturated water absorption rate of 120–150% of its own mass. After water absorption, it exhibits a radial expansion rate of approximately 8–10% and an axial expansion rate of approximately 2–3%, while maintaining good flexibility without significant disintegration. The fiber is a light-yellow powdery material with a length ranging from 1 mm to 3 mm. Its basic physical properties are summarized in Table 3.

Table 3. Physical properties of lignin fiber.

Density (g/cm^3)	Average Diameter (mm)	Length (mm)	Aspect Ratio /	Tensile Strength (MPa)	Modulus of Elasticity (GPa)
1.32	0.02	1–3	0.0067–0.02	220	20

2.2. Specimen Preparation

In this study, specimens were prepared using the wet tamping method. Following the preparation procedure described by Song et al. [35], ring knife specimens with a diameter of 61.8 mm and height of 20 mm, as well as cylindrical triaxial compression specimens with a diameter of 39.1 mm and height of 80 mm, were prepared.

During the preparation of the fiber–sand mixture, deaired water equivalent to 10% of the dry sand mass was first added. Lignin fiber was then added according to the target content, followed by the gradual addition of dry sand in multiple increments. The mixture was thoroughly mixed to prevent fiber separation from the sand skeleton and to ensure initial uniform fiber distribution.

For the cylindrical triaxial specimens, the fiber–sand mixture (for reinforced specimens) or moist sand (for plain sand specimens) was placed into the mold in four layers, with each layer controlled to a height of 20 mm and equal mass of the mixture. After each layer was compacted, the surface was scarified before the next layer was added, until the target height was achieved.

In the consolidation and rebound tests, to investigate deformation behavior under different initial states, specimens mixed at a moisture content of 10% were used as dry specimens, while saturated specimens were prepared by saturating the dry specimens prior to testing. Before testing, the saturation of the saturated specimens was ensured to be $S_r \geq 95\%$. The test procedure is illustrated in the flowchart shown in Figure 4.

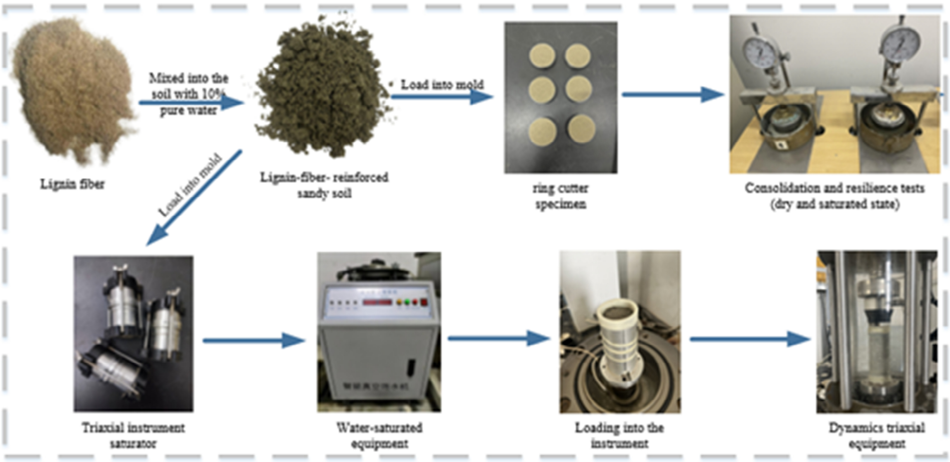

Figure 4. Flowchart of the experiment.

2.3. Pilot Program

2.3.1. Consolidation and Rebound Tests

The dry specimens were subjected to loading–unloading consolidation compression and resilient modulus tests using a consolidometer (Nanjing Soil Instrument Factory Co., Ltd., Nanjing, China). The applied pressure sequence was 25, 50, 100, 200, 400, 800, 400, 200, 100, 50, and 25 kPa, where the loading stages corresponded to the consolidation compression test and the unloading stages to the resilient modulus test.

2.3.2. Triaxial Compression Test

Consolidated–drained (CD) shear tests were conducted on specimens with different lignin fiber contents (FC) under confining pressures of 100, 200, and 300 kPa using a triaxial testing system. Given that the sandy soil used in this study is a fine sand with high permeability, and that shear rate has a minor effect on such permeable materials [37,38], a shear rate of 0.25%/min was adopted to save time and cost. The test was terminated when the axial strain reached 20%. The specimen dimensions were 39.1 mm in diameter and 80 mm in height.

To compare and analyze the effects of various influencing factors on the static properties of lignin fiber-reinforced sandy soil, consolidation and rebound tests were conducted under different fiber contents (FC) and vertical pressures (P), while triaxial compression tests were performed under different fiber contents (FC) and confining pressures (σ_3). The test programs are presented in Tables 4 and 5, respectively.

Table 4. Test program for consolidation and rebound of lignin-fiber-reinforced sandy soil.

Test Category	Fibre Content FC/%	Vertical Pressure P/kPa
Compression test Rebound test	0, 0.5, 1, 2, 3, 5	25, 50, 100, 200, 400, 800 800, 400, 200, 100, 50, 25

Table 5. Triaxial test program for lignin fiber reinforced sandy soil.

Test Group Number	Fibre Content FC/%	Confinement σ_3/kPa
1	0	100, 200, 300
2	0.5	
3	1	
4	2	
5	3	
6	5	

3. Analysis of Test Results

3.1. Consolidation Compression and Resilience Modulus Tests

3.1.1. Effect of Lignin Fiber Dosing on Compression and Resilience Curves

Through compression tests on sand reinforced with different lignin fiber contents (FC), the void ratios of the reinforced sand under various normal stresses were obtained, and the resulting relationship curves are shown in Figure 5. It can be observed from Figure 5 that the compression curves of sand with different FC under dry and saturated conditions exhibit significant differences.

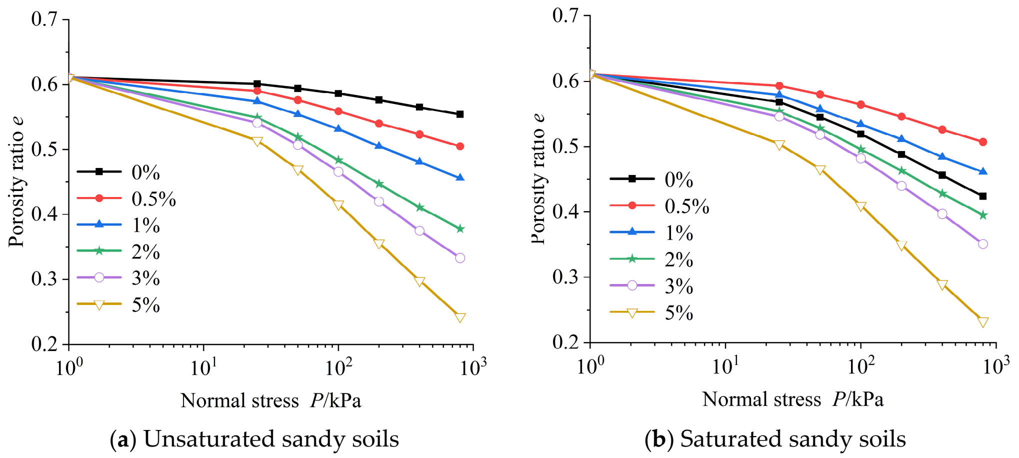

Figure 5. Effect of lignin fiber content FC on compression curves.

In the dry state, the *e*–lg*p* curve of the sand gradually shifts downward with increasing FC, indicating that under the same stress level, the void ratio decreases as the fiber content increases, yet the compression deformation and compressibility of the sand increase. This occurs because lignin fiber is a porous, lightweight material. When incorporated, it occupies part of the intergranular pore space, reducing the initial void ratio of the specimen. However, the fiber itself has a low modulus and high compressibility. Under external loading, the fiber undergoes significant compression deformation, which drives the overall compression of the sand. Consequently, although increasing FC reduces the initial void ratio, the high compressibility of the fiber dominates the deformation behavior of the soil, ultimately leading to an increase in compressibility with higher FC.

In the saturated state, the *e*–lg*p* curve of the sand initially shifts upward and then downward with increasing FC, with the smallest compression deformation observed at

FC = 0.5%. This is attributed to the properties of lignin fiber, which contains a large number of polar functional groups and exhibits a saturated water absorption rate of 120–150%. Upon water absorption, the fiber undergoes slight radial micro-expansion, which to some extent counteracts the compression induced by normal stress, thereby reducing the compression deformation of the sand. At FC = 0.5%, a small amount of fiber fills the pores and generates micro-expansion, resulting in a denser soil skeleton and reduced compressible pore space. When FC exceeds 0.5%, the excessive fiber content increases the contribution of fiber self-compression deformation, weakening the constraining effect of the pore structure. Consequently, the compressibility of the soil increases again, and the void ratio decreases more significantly with increasing load.

Figure 6 presents the void ratio versus pressure curves for the sandy soil in the rebound test. It can be observed that the variation patterns of the rebound curves for sand reinforced with different FC under dry and saturated conditions are essentially consistent. In all cases, a higher FC results in a greater increase in void ratio during rebound, and under the same pressure, the rebound curve becomes steeper as FC increases.

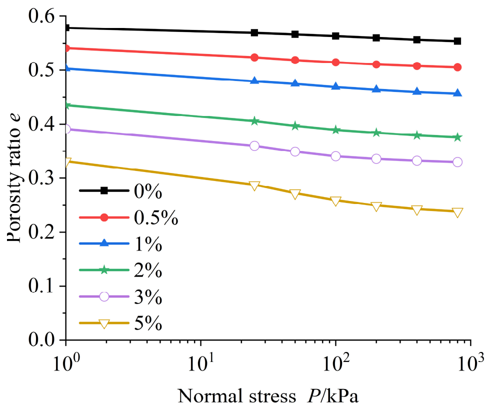

(**a**) Unsaturated sandy soils

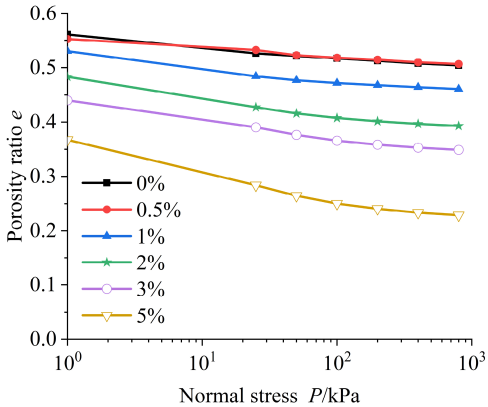

(**b**) Saturated sandy soils

Figure 6. Effect of lignin fiber content FC on resilience modulus *e*.

3.1.2. Effect of Fibre Dosage on Compression and Resilience Indicators

As shown in Figure 7, the compression coefficient a_v increases with increasing lignin fiber content (FC). Additionally, the negative correlation with water content results in a decrease in both the compression coefficient and compression index under saturated conditions. To further investigate the compressive properties of lignin fiber-reinforced sandy soil, the compression index C_c and rebound index C_s were selected for quantitative analysis within the pressure range of 100–200 kPa. Figure 8 presents the relationship curves between the compression index C_c and FC. With increasing FC, the compression index increases, while the values under saturated conditions are slightly lower than those in the dry state.

The continuous increase in sand compressibility with higher lignin fiber content arises from the combined effects of the fiber's inherent high compressibility and the flexible interlocking structure of the fiber–sand composite skeleton. The lignin fiber used in this study exhibits a porous, loosely networked microstructure at the microscopic level, characterized by weak intermolecular bonding forces. Under external normal stress, it is prone to plastic compression deformation, with its own compression accounting for 30–40% of the total compression deformation of the sand. This constitutes the direct cause of the increased compressibility of the sand.

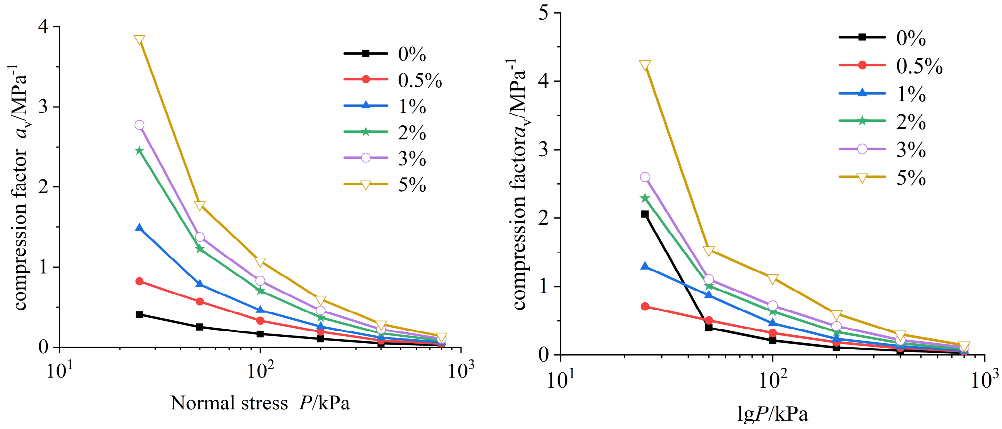

(**a**) Unsaturated sandy soils (**b**) Saturated sandy soils

Figure 7. Effect of lignin fiber content FC on resilience modulus *e*.

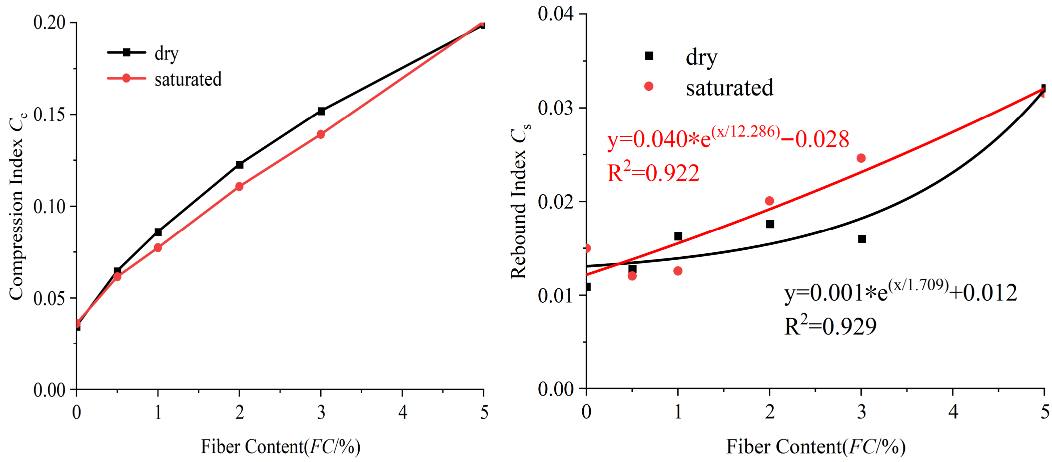

(**a**) Compression index (**b**) Rebound index

Figure 8. Effect of lignin fiber content FC on compression index of sandy soil.

Additionally, the flexible lignin fibers randomly distributed among the sand particles transform the soil skeleton from the rigid point-contact interlocking of plain sand into a flexible composite skeleton of "sand particles–fibers." Under loading, this facilitates coordinated deformation through fiber sliding and particle rearrangement, rather than relying on the rigid occlusal deformation resistance of plain sand particles. Moreover, the pore-filling effect of an appropriate amount of fiber does not completely eliminate the pore deformation space of the sand, ultimately resulting in the compression coefficient and compression index increasing monotonically with FC.

This trend is consistent with findings from studies on natural fiber-reinforced sand, such as straw fiber and hemp fiber, confirming that the flexible and high-compressibility characteristics of natural fibers commonly govern the compression deformation behavior of sand. In contrast, this behavior differs significantly from that of sand reinforced with synthetic fibers such as polypropylene and polyester. Due to their high modulus and low compressibility, the incorporation of synthetic fibers results in little to no change, or even a slight decrease, in sand compressibility, representing one of the key mechanical distinctions between natural fiber-reinforced and synthetic fiber-reinforced sand.

As shown in Figure 8, the variation pattern of the rebound index under different dry and saturated conditions can be more clearly observed through fitting and comparison. The difference between the two conditions decreases with increasing fiber content, and the rebound index under saturated conditions is slightly higher than that under dry conditions.

Furthermore, as the lignin fiber content increases, the effect of moisture content on the differences in compression and rebound indices gradually diminishes. When FC reaches 5%, the influence of dry and wet conditions on these indices becomes negligible, essentially no longer having an effect. This is because the continuous fiber network formed by a high content of lignin fiber can counteract the weakening effect of water on interparticle bonding in sand under saturated conditions. Additionally, the volume stability of the fiber after water absorption results in consistent deformation characteristics of the soil skeleton under both dry and saturated conditions, ultimately eliminating the influence of moisture content on the compression and rebound indices.

3.2. Triaxial Compression Test Results

3.2.1. Effect of FC on Stress–Strain Characteristics

Figure 9 presents the stress–strain relationship curves of lignin fiber-reinforced sandy soil under the same confining pressure σ_3 and varying fiber contents (FC). The following observations can be made: (1) The stress–strain curves of sandy soil reinforced with different FC all exhibit nonlinear characteristics. (2) Under a given confining pressure, FC significantly influences the shape of the stress–strain curve. At the initial stage of loading, the axial strain is small, and the deviatoric stress increases rapidly with axial strain, quickly reaching a peak value. As the axial strain continues to increase, the deviatoric stress gradually decreases, albeit at a slow rate, indicating that the fiber-reinforced sandy soil retains a certain residual strength after peak failure, exhibiting strain-softening behavior. (3) With increasing FC, the stress–strain curve initially shifts upward and then downward. Under lower confining pressures, the curve for FC = 3% is positioned at the top, whereas under higher confining pressures, the curve for FC = 5% is positioned at the top. (4) The morphological characteristics of the stress–strain curves change significantly with increasing FC. At a confining pressure of 300 kPa, FC has a more pronounced effect on the curve morphology, which gradually transitions from strain-softening to strain-hardening behavior as FC increases.

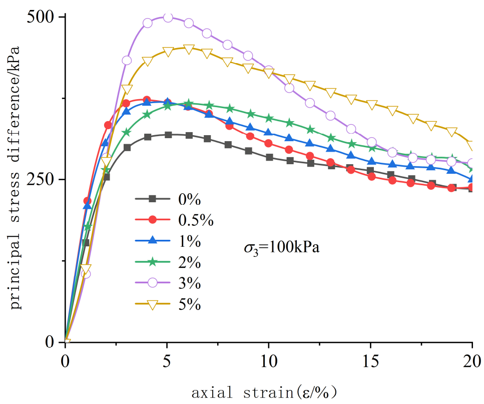

(**a**) σ_3 = 100 kPa

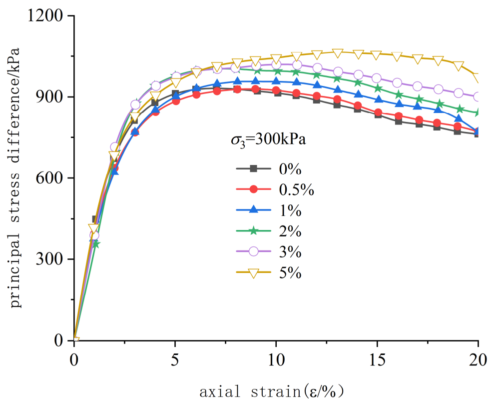

(**b**) σ_3 = 300 kPa

Figure 9. Effect of lignin fiber dosing *FC* on stress–strain curve of sandy soil.

This evolution of stress–strain behavior is essentially the result of the coupled effects of fiber reinforcement and fiber accumulation, which are governed by fiber content and confining pressure. At low fiber content, the reinforcement effect of uniformly distributed fibers dominates, with fiber bridging and interfacial friction enhancing the shear strength of the soil. At high fiber content, the accumulation effect of fibers gradually becomes apparent. However, when the confining pressure is sufficiently high, it can compact the accumulated fibers, allowing them to regain their interlocking and reinforcing functions, ultimately enabling the transition from strain softening to strain hardening.

https://doi.org/10.3390/buildings16081532

Considering the porous and loose microstructure of lignin fiber, the fiber–sand interfacial interaction mechanisms, and the experimental observations, this coupled regulation mechanism can be further detailed as follows. At low fiber content (FC $\leq$ 3%), the fibers are uniformly dispersed among the sand particles without agglomeration. Their rough surfaces establish good interfacial friction with the sand particles, while the fibers connect adjacent sand particles through a bridging effect, restricting particle sliding and rolling, and enhancing the internal interlocking capacity of the soil. This increases the shear strength of the soil and shifts the stress–strain curve upward. Moreover, due to the flexible buffering effect of the fibers, the deviatoric stress decreases gently after the peak, maintaining a certain residual strength.

At high fiber content (FC > 3%) under low confining pressure, excessive fibers tend to agglomerate, reducing the direct contact area between sand particles and creating weak planes within the soil. This limits the increase in shear strength, and the stress–strain curve shifts slightly downward. Under high confining pressure (e.g., 300 kPa), however, the external pressure compacts the agglomerated fibers, re-establishing close contact between fibers and sand particles and forming a continuous fiber–sand load-bearing system. At this stage, the reinforcement effect of the fibers again becomes dominant, not only increasing the peak strength of the soil but also altering its deformation characteristics. As a result, the stress–strain curve transitions from strain softening to strain hardening—meaning that as axial strain increases, the deviatoric stress no longer decreases significantly but instead continues to rise slightly. This occurs because the compacted fibers and sand particles form a more stable load-bearing structure capable of sustaining greater shear deformation.

The regulating role of confining pressure is equally indispensable. A higher confining pressure imposes stronger constraints on both fibers and sand particles. On one hand, it compacts fiber agglomerates, enhancing the reinforcement effect of the fibers; on the other hand, it restricts the lateral displacement of sand particles, reducing strength loss due to particle rearrangement. Therefore, under high confining pressure, the reinforcement effect of high fiber content (FC = 5%) becomes more pronounced, with the stress–strain curve positioned at the top and exhibiting more distinct strain-hardening characteristics. This trend is consistent with findings from studies on polypropylene fiber-reinforced sand by Zhao et al. (2020) [16] and coconut fiber-reinforced red clay by Yang et al. (2023) [18], all of which confirm that the coupling between fiber content and confining pressure is a key factor in regulating the stress–strain behavior of soil.

3.2.2. Effect of Circumferential Pressure on Stress–Strain

As shown in Figure 10: (1) Confining pressure significantly influences the stress–strain relationship of sandy soil, with the curves shifting upward as confining pressure increases. For a fixed fiber content (FC), the peak strength of the specimen exhibits a positive correlation with confining pressure—that is, an increase in confining pressure leads to higher peak strength. As the confining pressure increases, the slope of the initial linear segment of the stress–strain curve also increases. Within the same strain interval, the difference in deviatoric stress at a confining pressure of 300 kPa is substantially greater than that at 200 kPa and 100 kPa. This indicates that a higher vertical stress is required to induce failure in the specimen at a confining pressure of 300 kPa compared to the lower confining pressure cases. Therefore, an increase in confining pressure enhances the soil's resistance to shear failure. (2) Under various confining pressure conditions, the stress–strain curves of sandy soil with different FC generally exhibit strain-softening behavior. However, the degree of softening decreases as confining pressure increases, as evidenced by the larger axial strain required to reach the peak stress for each FC under higher confining pressures. At FC = 5%, the stress–strain curves at confining pressures of 100 kPa and 200 kPa show a clear trend toward hardening compared with those at other fiber contents. At a confining pressure of 300 kPa, the stress–strain curve exhibits a hardening-type behavior.

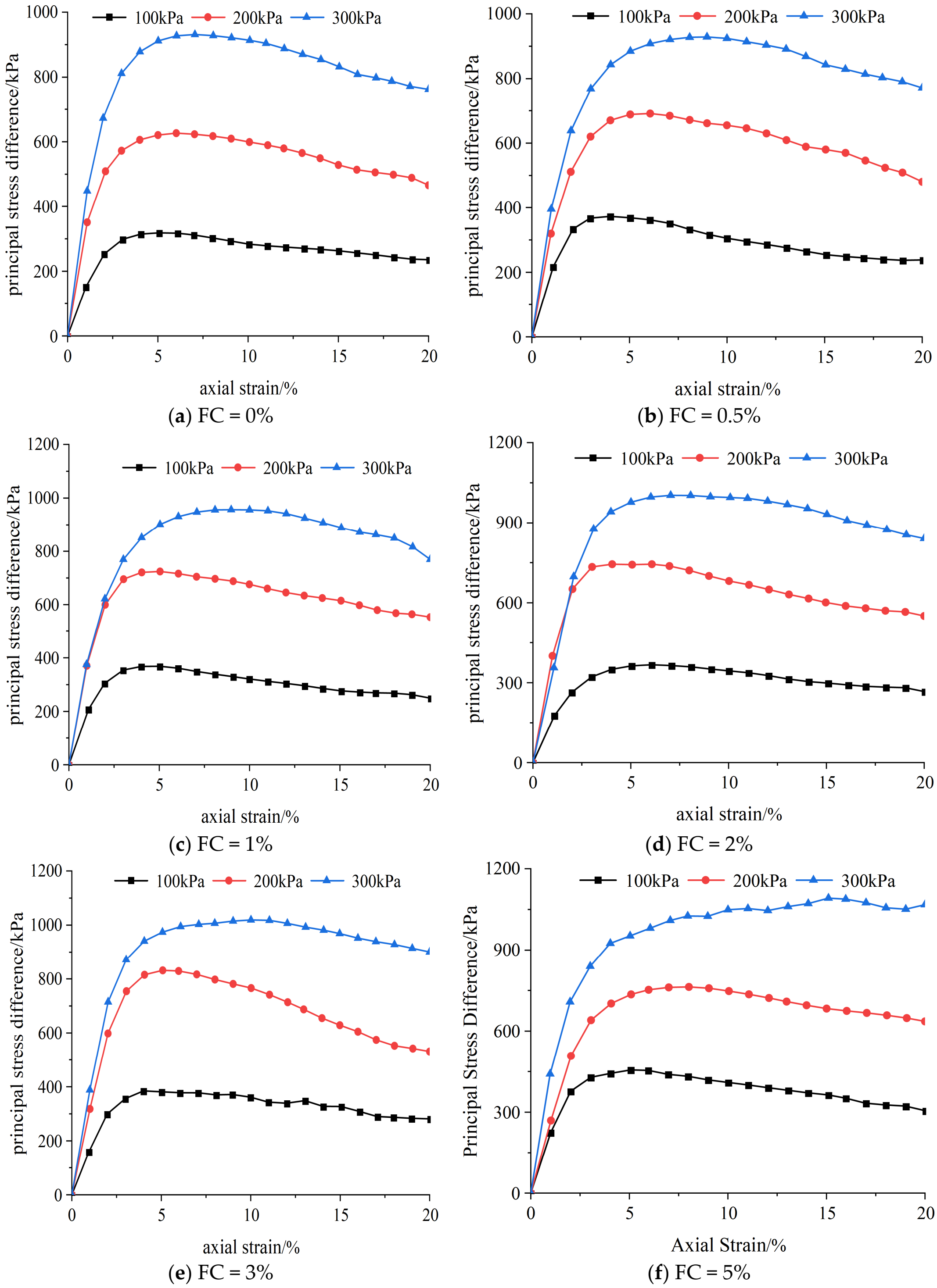

Figure 10. Effect of circumferential pressure σ3 on stress–strain curves of sandy soil under different FC.

The suppression of the softening degree and the promotion of the hardening transition by confining pressure arise from the compaction and constraint effects that high confining pressure exerts on the fiber–sand skeleton. High confining pressure facilitates closer contact between sand particles and fibers and enhances interparticle interlocking and fiber interfacial friction, while also constraining volumetric deformation during shearing and reducing strength attenuation caused by dilatancy. For specimens with high fiber content, high confining pressure effectively compacts fiber accumulation zones, eliminates internal defects induced by fiber agglomeration, allows the network reinforcement effect of high-content fibers to be fully utilized, and ultimately achieves a hardening-type stress–strain curve.

3.2.3. Effect of Fibre Doping on Volumetric Strain

Specify that the volumetric strain ε_v is positive for volumetric expansion ($\varepsilon_v > 0$) and negative for volumetric compression ($\varepsilon_v < 0$). The volumetric strain ε_v~axial strain ε_a curves of lignin fiber-reinforced sandy soil under the same confining pressure σ_3 and different lignin fibre admixture *FC* conditions are shown in Figure 11. As can be seen from Figure 11: (1) When the circumferential pressure σ_3 is certain, the volumetric strain ε_v first increases and then gradually decreases with the increase in fibre doping FC. (2) At lower peripheral pressures σ_3 (σ_3 of 100 kPa and 200 kPa), the shear expansion characteristics gradually increase with increasing fibre incorporation FC. It is shown that lignin fibres enhance the shear expansion characteristics of sandy soils due to the fact that lignin fibres fill the inter-pore spaces between sandy soil particles and make the bond between sandy soil particles larger, which increases the resistance to particle rearrangement but decreases the shear expansion characteristics of sandy soils as FC continues to increase. (3) At low peripheral pressure σ_3, lower or higher fibre doping will allow the specimen to exhibit shear shrinkage.

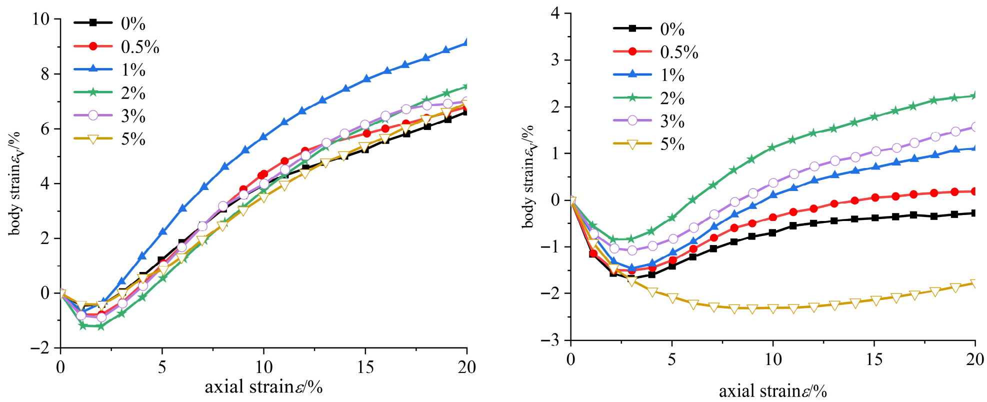

(**a**) σ_3 = 100 kPa (**b**) σ_3 = 300 kPa

Figure 11. Effect of different fiber content FC on the volumetric strain–axial strain relationship curve.

Figure 12 presents the volumetric strain ε_v versus axial strain ε_a curves of lignin fiber-reinforced sandy soil under the same fiber content (FC) and varying confining pressures σ_3. The following observations can be made:

(1) For a given FC, the volumetric strain ε_v decreases with increasing σ_3 across all FC ranges. (2) At low FC, the volumetric deformation of lignin fiber-reinforced sandy soil under high confining pressure exhibits shear contraction. This is because sandy soil has a low dry density and large pore space. At low FC, lignin fibers fill only a small portion of the intergranular pores, and the void ratio remains relatively large. Under high confining pressure, particles are gradually rearranged to achieve a denser state, resulting in shear contraction behavior. (3) As FC increases, the volumetric deformation of sandy soil under high confining pressure gradually transitions from shear contraction to shear expansion. This occurs because, when FC reaches a certain level, lignin fibers fill most of the intergranular pores, leading to a denser soil structure with a smaller void ratio. During shearing, particle rearrangement disrupts this denser structure, giving rise to shear expansion characteristics.

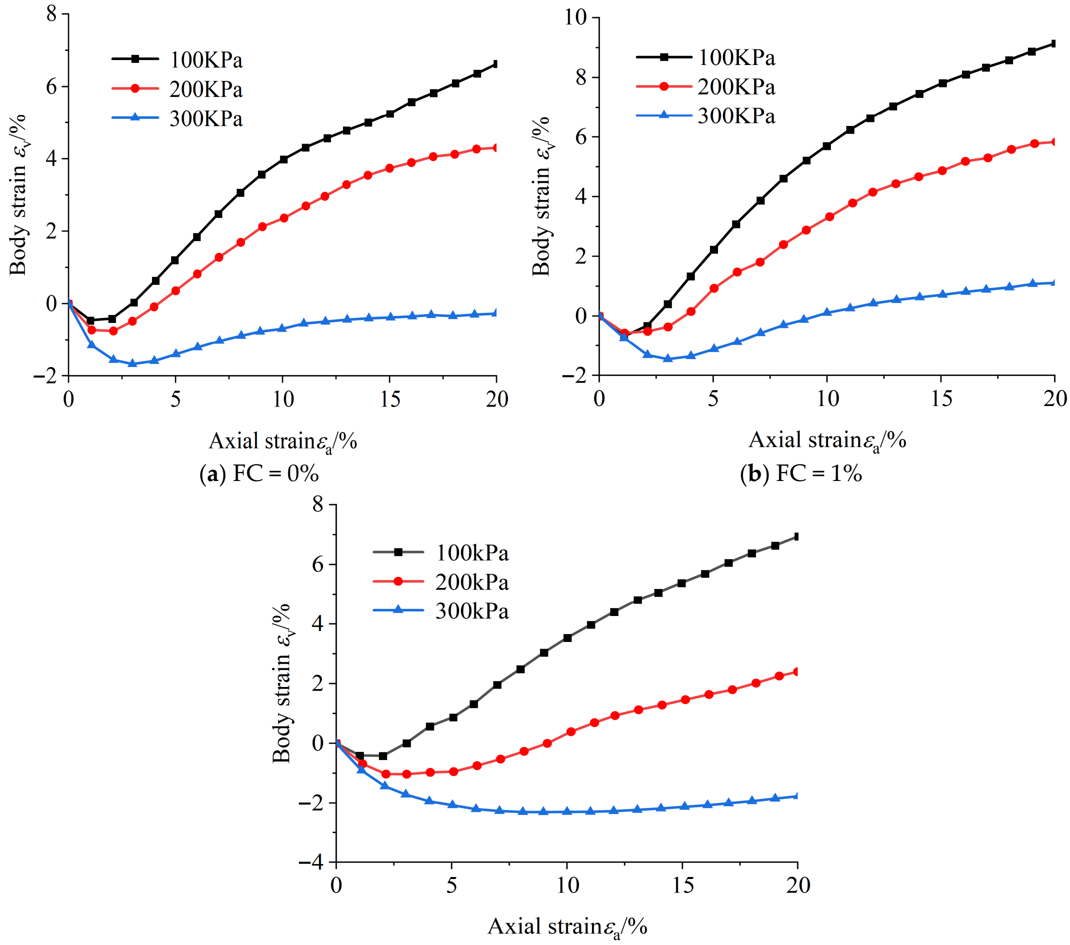

(**a**) FC = 0% (**b**) FC = 1%
(**c**) FC = 5%

Figure 12. Effect of different fiber content FC on the volumetric strain–axial strain relationship curve.

However, with further increases in FC, shear expansion begins to revert to shear contraction. This can be attributed to the results of the rebound tests, which indicate that the incorporation of lignin fibers increases the compressibility of sandy soil. A higher FC makes the soil more susceptible to compression under high confining pressure, thereby suppressing dilatancy.

The regulation of sand strain by lignin fiber is closely related to the fiber's pore-filling effect and its inherent compressibility characteristics. An appropriate amount of fiber filling increases soil compactness, resulting in greater resistance to particle rearrangement during shearing and enhanced dilatancy characteristics. Conversely, excessive fiber accumulation, combined with the fiber's high compressibility, makes the soil prone to volume compression under the combined action of shearing and high confining pressure, thereby weakening dilatancy or even leading to contraction.

This pattern is consistent with the volumetric strain evolution observed in sand reinforced with natural fibers such as hemp fiber and straw fiber. In contrast, synthetic fibers, due to their low compressibility, can maintain strong dilatancy characteristics even at high contents, further highlighting the differences between natural and synthetic fibers in regulating soil volumetric deformation.

From a microstructural perspective, the transition from dilatancy to contraction is closely related to the fiber filling effect, the evolution of pore structure, and the inherent compressibility of the fiber itself. When the fiber content is low, lignin fibers only partially fill the interparticle pores, and the soil skeleton is dominated by sand particle contacts, resulting in relatively low compactness. During shearing, sand particles tend to float, rotate, and rearrange, manifesting macroscopically as significant dilatancy.

As the fiber content increases, lignin fibers form a network structure within the sand. This network, on one hand, increases the initial compactness of the soil; on the other hand, the fibers themselves exhibit microstructural characteristics such as porosity, looseness, low modulus, and high compressibility. Under the combined action of shearing and confining pressure, the fibers undergo compression deformation, and the original pores are compacted and closed, allowing sand particles to move into the compressed pore space. This inhibits the development of dilatancy, causing the soil to gradually transition from dilatancy to contraction.

Under high confining pressure, external constraints further limit the lateral movement and upward floating of sand particles, reinforcing the fiber compression and pore compaction effects, thereby accelerating the transition from dilatancy to contraction. This microstructural evolution mechanism is consistent with the macroscopic volumetric strain behavior, collectively revealing the regulatory role of fiber content and confining pressure in the dilatancy–contraction transition.

3.2.4. Effect of FC on Strength Indicators

As shown in Figure 13, the lignin fiber content (FC) significantly influences the cohesion and internal friction angle of sand. With increasing FC, cohesion exhibits a continuous upward trend, reaching a peak value of 26.3 kPa. The internal friction angle, however, initially increases and then decreases, peaking at 33.7° when FC = 2%. Lignin fibers substantially enhance cohesion, whereas their effect on the internal friction angle is characterized by an optimal content—a feature closely related to the microscopic interaction mechanisms between fibers and sand.

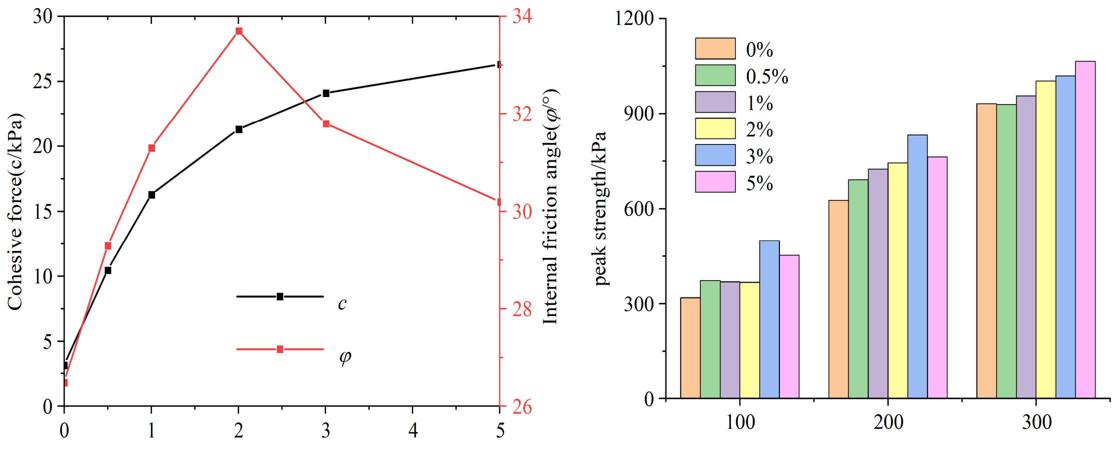

(**a**) Cohesion and angle of internal friction (**b**) Peak strength

Figure 13. Effect of lignin fiber content FC on strength parameters.

The initial increase and subsequent decrease in the internal friction angle essentially reflect the interplay between the fiber interlocking reinforcement effect and the accumulation weakening effect as the fiber content varies.

In the low-content stage (FC $\leq$ 2%), lignin fibers—characterized by rough surfaces, micropores, and uniform distribution—restrict the sliding and rolling of sand particles through fiber bridging, thereby enhancing interparticle interlocking and occlusal interactions. Meanwhile, the interfacial sliding friction between fibers and sand particles adds to the inherent friction among sand particles, significantly improving the overall shear friction resistance of the soil. As a result, the internal friction angle gradually increases with increasing FC. This trend is consistent with findings reported by Zhao et al. (2020) on polypropylene fiber-reinforced sand [16] and by Yang et al. (2023) on coconut fiber-reinforced red clay [18], both confirming that an appropriate amount of fibers can enhance the internal friction angle of soils through physical interlocking and interfacial friction.

The threshold value (FC = 2%) obtained in this study is similar to that reported by Ma et al. (2018) for coir fiber-reinforced sand [39], where the optimal coir fiber content was approximately 1.2%, and excessive content similarly weakened the reinforcement due to fiber accumulation. This similarity suggests that the threshold for improving the internal friction angle in fine sand systems is comparable for natural fibers and is primarily governed by sand particle gradation and fiber morphology (length and specific surface area). In this study, lignin fibers are short fibers with lengths of 1–3 mm and a large specific surface area, allowing pore filling and uniform distribution at a low content; therefore, the threshold is slightly lower than that for longer natural fibers.

In the high-content stage (FC > 2%), the pores among sand particles are already sufficiently filled by fibers. Excess fibers tend to form aggregates and accumulations, significantly reducing the direct contact area between sand particles and weakening the inherent interlocking and occlusal interactions. Moreover, the accumulated fibers are prone to self-sliding under shear, forming weak friction surfaces within the soil. The sliding friction resistance of these weak surfaces is much lower than the interlocking friction among sand particles, ultimately leading to a decreasing trend in the internal friction angle.

The continuous increase in cohesion with FC is primarily attributed to the chemical adsorption characteristics and network-like cementation structure of lignin fibers. For unreinforced sand, poor gradation results in large interparticle voids and nearly negligible cohesion. Lignin fibers contain polar functional groups such as hydroxyl and methoxy groups, which can form physical adsorption forces with sand particle surfaces. As fiber content increases, fibers gradually form a continuous network structure within the sand, establishing a “fiber cementation network” that wraps and connects sand particles, continuously improving the bonding characteristics of the soil.

This behavior differs significantly from that of synthetic fiber-reinforced sand. Synthetic fibers, with their nonpolar molecular structures, exhibit negligible adsorption with sand particles and primarily enhance the internal friction angle through reinforcement mechanisms, resulting in minimal improvement in cohesion. In contrast, natural fibers such as lignin fibers, by virtue of their polar functional groups and network-forming ability, serve as efficient and environmentally friendly materials for enhancing the cohesion of sandy soils, representing a key advantage of natural fibers in the reinforcement of low-cohesion sands.

As shown in Figure 13b, the peak strength initially increases and then decreases with increasing FC. Confining pressure exhibits a positive correlation with peak strength: a higher confining pressure results in denser soil, greater peak strength, and enhanced resistance to shear failure. The variation in peak strength is the result of the synergistic effects of cohesion and internal friction angle. At low fiber contents, both parameters increase, leading to a continuous rise in peak strength. At high fiber contents, the decrease in internal friction angle is less pronounced than the increase in cohesion, so the peak strength declines at a relatively slow rate. Under high confining pressure, however, the peak strength continues to increase with FC due to enhanced particle interlocking and fiber compaction. This indicates that confining pressure plays a more dominant role in regulating the strength improvement of lignin fiber-reinforced sand.

https://doi.org/10.3390/buildings16081532

4. Modification of the Duncan Chang Model

The Duncan–Chang model can effectively describe the deformation behavior of soil under triaxial compression [40,41]; however, it is limited to fitting the pre-peak stage of the stress–strain curve and cannot capture the strain-softening characteristics that occur after the peak. Furthermore, existing modified models predominantly focus on single-parameter optimization for specific types of improved soils [16–18] and are not suitable for the dynamic mechanical behavior of lignin fiber-reinforced sand, which exhibits softening under low confining pressure and hardening under high confining pressure. Additionally, these models overlook the unique interaction mechanisms between fibers and sand, and their direct application would result in significant fitting deviations.

Kondner, through triaxial compression tests on various soil materials, found that the relationship curve of $\sigma_1 - \sigma_3 \sim \varepsilon$ exhibits pronounced hyperbolic characteristics. The generalized relationship is expressed in Equation (1):

$$\sigma 1 - \sigma 3 = \frac{\varepsilon}{a + b\varepsilon} \tag{1}$$

where a, b are fitting parameters.

For strain-hardening stress–strain curves, the parameters a and b can be better fitted using the Duncan-Chang model. For strain softening type curves, the Duncan-Chang model is not fitted with high accuracy. For this reason, this paper proposes a modified Duncan-Chang model based on the Duncan-Chang model that can reflect the strain softening characteristics of the material, and its expression is:

$$\sigma 1 - \sigma 3 = \frac{\varepsilon}{m + n\varepsilon + l\varepsilon^2} \tag{2}$$

Among them:

$$m = \frac{1}{E_0}$$

$$n = \frac{1}{(\sigma 1 - \sigma 3)_f} - \frac{2}{\varepsilon_{1f} E_0}$$

$$l = \frac{1}{E_0 \varepsilon_{1f}^2}$$

where E_0 is the initial modulus of elasticity and ε_{1f} is the strain value corresponding to the peak deviatoric stress.

For the conventional triaxial test, the initial modulus of elasticity of the specimen is equal to the initial tangential modulus at the starting point of the test (ε_1 = 0) [42]. The initial tangent modulus of the specimen can be obtained as:

$$\left[\frac{d(\sigma 1 - \sigma 3)}{d\varepsilon_1}\right]_{\varepsilon 1 = 0} = \frac{a}{(a + b\varepsilon_1)^2}\bigg|_{\varepsilon 1 = 0} = \frac{1}{a} \tag{3}$$

From this, the initial modulus of elasticity E_0 is obtained as

$$E_0 = \frac{1}{a} \tag{4}$$

The fitting parameters m, n and l of the modified Duncan-Chang model under the corresponding conditions can be obtained from the above equation and are shown in Table 6.

Table 6. Correction of Duncan-Chang model fitting parameters.

FC/%	σ_3/kPa	m/(10^{-3} kPa)	n/(10^{-3} kPa)	l/(10^{-5} kPa)
0	100	3.189	2.055	9.569
	200	1.478	1.118	3.470
	300	1.152	0.758	2.090
0.5	100	2.958	1.258	16.200
	200	1.806	0.835	4.920
	300	1.296	0.768	1.810
1	100	1.917	1.733	11.200
	200	0.908	0.944	4.400
	300	1.597	0.645	2.440
2	100	3.047	1.527	10.300
	200	1.270	0.920	2.917
	300	1.282	0.755	1.040
3	100	3.933	1.474	7.620
	200	1.580	0.570	6.120
	300	1.383	0.657	1.570
5	100	2.509	1.191	9.780
	200	1.897	0.831	2.860
	300	1.387	0.696	0.797

Under different testing schemes, a comparison of the measured stress–strain curves of lignin fiber-reinforced sand, the theoretical curves of the modified Duncan–Chang model, and the curves of the original Duncan–Chang model is presented in Figure 14. To quantitatively evaluate the fitting accuracy of the three models, the coefficient of determination (R^2), root mean square error (RMSE), and mean absolute error (MAE) were calculated based on the test data under all working conditions. The comparison results are summarized in Table 7.

As shown in Figure 13 and Table 7, the traditional Duncan–Chang model can only reasonably simulate the stress–strain behavior before failure and fails to capture the strain-softening characteristics after the peak. The early fiber-reinforced soil improvement model exhibits the same limitation. When the stress exceeds the peak strength, the calculated results of both models deviate significantly from the measured results, which is quantitatively reflected by average R^2 values of only 0.887 and 0.924, and RMSE values as high as 18.62 kPa and 12.37 kPa. In contrast, the modified Duncan–Chang model proposed in this study, through the innovative introduction of core parameters and the construction of a dynamic parameter system, achieves high-precision fitting both before and after the peak. The average R^2 reaches 0.986, with RMSE and MAE of only 3.15 kPa and 2.48 kPa, respectively. Notably, under conditions with significant strain softening at low confining pressure, it still maintains a high fitting accuracy with R^2 = 0.981, effectively addressing the insufficient accuracy of existing models and achieving a remarkably significant improvement in prediction accuracy.

The high-precision fitting of this model is essentially attributed to the strong alignment between its modification mechanism and the mechanical behavior of lignin fiber-reinforced sand. By anchoring the peak point with ε_{1f} and optimizing the initial deformation with E_0, it accurately captures the core characteristics of strain softening in the fiber–sand system. Meanwhile, the dynamic parameter system quantifies the coupled effects of fiber content and confining pressure, enabling the model to adapt to variations in mechanical behavior under different working conditions.

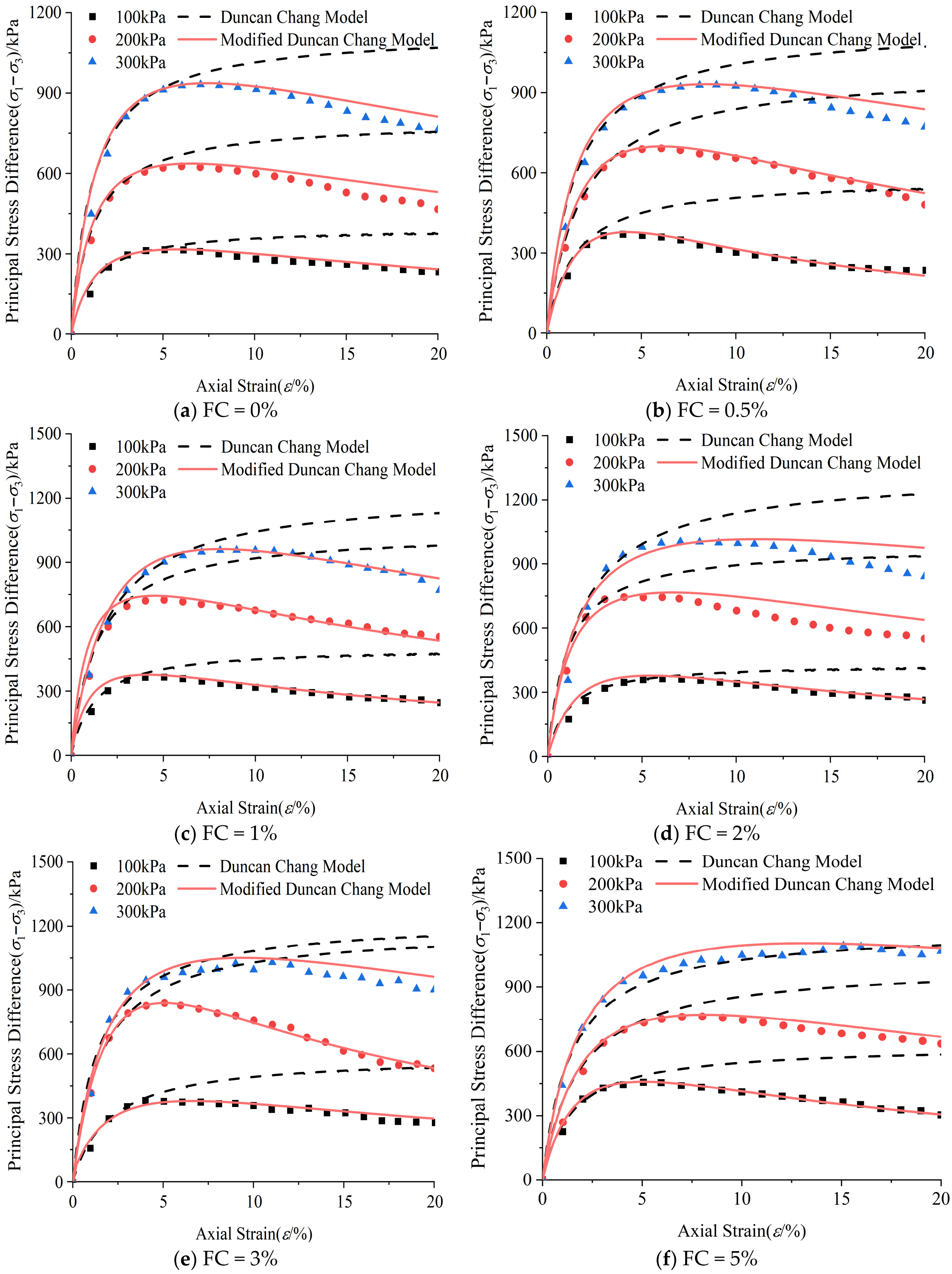

Figure 14. Comparison of Duncan–Chang and its modified model with measured results.

Table 7. Quantitative comparison of fitting accuracy of different models.

Model Type	Mean Determination Coefficient	Root Mean Square Error (kPa)	Mean Absolute Error (kPa)
Traditional Duncan–Chang model	0.887	18.62	14.25
Early Fiber-Reinforced Soil Improvement Model	0.924	12.37	9.71
Correcting the Duncan–Chang model	0.986	3.15	2.48

5. Conclusions

This paper investigates the stress–strain and volumetric strain behavior of sand reinforced with different lignin fiber contents (*FC*) through compression, consolidation, and triaxial compression tests. Based on the Duncan–Chang model, a modified analysis is conducted and compared. The main conclusions are as follows:

(1) The incorporation of fibers increases the compressibility and rebound amount of sandy soil. The higher the fiber content, the more compressible the soil and the more pronounced the rebound. Water immersion has a certain deteriorating effect on compression and rebound, but increasing the fiber content can effectively weaken this effect.

(2) Under a given confining pressure, the fiber content significantly affects the shape of the stress–strain curve of sandy soil. As the confining pressure increases, the curves for all fiber contents gradually transition from strain softening to strain hardening.

(3) The cohesion increases continuously with increasing fiber content, while the internal friction angle first increases and then decreases. The enhancing effect of fibers on cohesion is significantly better than their influence on the internal friction angle.

(4) The peak strength is positively correlated with both fiber content and confining pressure. It increases significantly with higher confining pressure, and also improves with increasing fiber content under high confining pressure. Overall, the effect of confining pressure on peak strength is more pronounced.

(5) The modified Duncan–Chang model proposed in this paper introduces the peak strain ε_{1f} and the initial elastic modulus E_0, establishing a dynamic parameter system that couples fiber content and confining pressure. This model effectively captures the strain-softening behavior of sand reinforced with lignin fiber and demonstrates good agreement with the measured data.

(6) In water conservancy projects in western China, when lignin fiber is used to reinforce poorly graded fine sand, the fiber content should be controlled within 1% to 2%, which can achieve a balance between strength enhancement and deformation control. As a recycled solid waste material, lignin fiber is both environmentally friendly and economical, offering a feasible technical solution for the reinforcement of sandy soil foundations.

Author Contributions: H.Y.: Conceptualization, Methodology, Writing—Review and Editing; Y.A.: Software, Validation, Investigation; Y.S.: Formal analysis, Writing—Original Draft; K.Y.: Resources, Data Curation; C.C.: Supervision, Funding acquisition; G.Z.: Project administration, Visualization. All authors have read and agreed to the published version of the manuscript.

Funding: This work was supported by the "Tianshan Talents" Science and Technology Innovation Leading Talent Program in Xinjiang Uygur Autonomous Region [2024TSYCLJ0017]; National Natural Science Foundation of China [42462030]; Key Laboratory of Dam Construction Safety and Disaster Prevention of Xinjiang Production and Construction Corps [TC202501004].

Data Availability Statement: The original contributions presented in this study are included in the article. Further inquiries can be directed to the corresponding author.

Conflicts of Interest: Author Haihua Yang was employed by the company, Key Laboratory of Dam Construction Safety and Disaster Prevention of Xinjiang Production and Construction Corps. And author Chaohong Chen was employed by the company Key Laboratory of Dam Construction Safety and Disaster Prevention of Xinjiang Production and Construction Corps and XPCC Surveying & Designing Institute Group Co., Ltd. The remaining authors declare that the research was conducted in the absence of any commercial or financial relationships that could be construed as a potential conflict of interest. The authors declare that they have no known competing financial interests or personal relationships that could have appeared to influence the work reported in this paper. Haihua Yang and Chaohong Chen are employees of Key Laboratory of Dam Construction Safety and Disaster Prevention of Xinjiang Production and Construction Corps, who provided funding and teachnical support for the work. The funder had no role in the design of the study; in the collection, analysis, or interpretation of data, in the writing of the manuscript, or in the decision to publish the results.

References

1. Yan, F.; Wu, B.; Wang, Y. Estimating spatiotemporal patterns of aboveground biomass using Landsat TM and MODIS images in the Mu Us Sandy Land, China. *Agric. For. Meteorol.* **2015**, *200*, 119–128. [CrossRef]
2. Li, X.Y.; Liu, L.Y.; Wang, J.H. Wind tunnel simulation of aeolian sandy soil erodibility under human disturbance. *Geomorphology* **2004**, *59*, 3–11. [CrossRef]
3. Sato, A.; Kawasaki, S.; Hata, T.; Hayashi, T. Possibility for solidification of peaty soil by using microbes. *GEOMATE J.* **2016**, *10*, 2071–2076. [CrossRef]
4. Bordoloi, S.; Garg, A.; Sekharan, S. A review of physio-biochemical properties of natural fibers and their application in soil reinforcement. *Adv. Civ. Eng. Mater.* **2017**, *6*, 323–359. [CrossRef]
5. Rajak, D.K.; Pagar, D.D.; Menezes, P.L.; Linul, E. Fiber-Reinforced Polymer Composites: Manufacturing, Properties, and Applications. *Polymers* **2019**, *11*, 1667. [CrossRef]
6. Pujari, S.; Ramakrishna, A.; Padal, K.T.B. Comparison of ANN and regression analysis for predicting the water absorption behaviour of jute and banana fiber reinforced epoxy composites. *Mater. Today Proc.* **2017**, *4*, 1626–1633. [CrossRef]
7. Vidal, H. The principle of reinforced earth. *Highw. Res. Rec.* **1969**, *282*, 1–16.
8. Lekha, B.M.; Goutham, S.; Shankar, A.U.R. Evaluation of lateritic soil stabilized with Arecanut coir for low volume pavements. *Transp. Geotech.* **2015**, *2*, 20–29. [CrossRef]
9. Bordoloi, S.; Hussain, R.; Garg, A.; Sreedeep, S.; Zhou, W.H. Infiltration characteristics of natural fiber reinforced soil. *Transp. Geotech.* **2017**, *12*, 37–44. [CrossRef]
10. Yang, Y.; Liu, H.; Lin, B.; Tang, D.; Xu, J.; Dai, L.; Si, C. From biomass to vitrimers: Latest developments in the research of lignocellulose, vegetable oil, and naturally-occurring carboxylic acids. *Ind. Crops Prod.* **2023**, *206*, 117690. [CrossRef]
11. Fagone, M.; Loccarini, F.; Ranocchiai, G. Strength evaluation of jute fabric for the reinforcement of rammed earth structures. *Compos. Part B Eng.* **2017**, *113*, 1–13. [CrossRef]
12. Ibrahim, M.M.; Dufresne, A.; El-Zawawy, W.K.; Agblevor, F.A. Banana fibers and microfibrils as lignocellulosic reinforcements in polymer composites. *Carbohydr. Polym.* **2010**, *81*, 811–819. [CrossRef]
13. Sharma, V.; Vinayak, H.K.; Marwaha, B.M. Enhancing compressive strength of soil using natural fibers. *Constr. Build. Mater.* **2015**, *93*, 943–949. [CrossRef]
14. Satyanarayana, K.G.; Arizaga, G.G.C.; Wypych, F. Biodegradable composites based on lignocellulosic fibers—An overview. *Prog. Polym. Sci.* **2009**, *34*, 982–1021. [CrossRef]
15. Peng, W.; Wang, Q.; Liu, Y.; Sun, X.; Chen, Y.; Han, M. The influence of freeze-thaw cycles on the mechanical properties and parameters of the Duncan-chang constitutive model of remolded saline soil in Nong'an County, Jilin Province Northeastern China. *Appl. Sci.* **2019**, *9*, 4941. [CrossRef]
16. Zhao, Y.; Ling, X.; Gong, W.; Li, P.; Li, G.; Wang, L. Mechanical properties of fiber-reinforced soil under triaxial compression and parameter determination based on the Duncan-Chang model. *Appl. Sci.* **2020**, *10*, 9043. [CrossRef]
17. He, J.; Gao, P.; Yang, H.; Tian, W.; Ding, J. Triaxial testing and model study on lime modified dispersive soil considering age effects. *Bull. Eng. Geol. Environ.* **2024**, *83*, 456. [CrossRef]
18. Yang, H.; Li, P.; Yang, E.; Jiang, X.; Chen, J. The strength law of coir fiber-reinforced soil based on modified Duncan-Chang model. *Front. Earth Sci.* **2023**, *10*, 1078624. [CrossRef]
19. Ghosh, S.K.; Bhattacharyya, R.; Mondal, M.M. Potential applications of open weave jute geotextile (soil saver) in meeting geotechnical difficulties. *Procedia Eng.* **2017**, *200*, 200–205. [CrossRef]

20. Narani, S.; Abbaspour, M.; Hosseini, S.; Nejad, F.M. Long-term dynamic behavior of a sandy subgrade reinforced by Waste Tire Textile Fibers (WTTFs). *Transp. Geotech.* **2020**, *24*, 100375. [CrossRef]
21. Diambra, A.; Ibraim, E.; Russell, R.A.; Muir Wood, D. Fibre reinforced sands: From experiments to modelling and beyond. *Int. J. Numer. Anal. Methods Geomech.* **2013**, *37*, 2427–2455. [CrossRef]
22. Zafar, T.; Ansari, M.; Husain, A. Soil stabilization by reinforcing natural and synthetic fibers—A state of the art review. *Mater. Today Proc.* 2023, *in press*. [CrossRef]
23. Salih, M.M.; Osofero, I.A.; Imbabi, S.M. Constitutive models for fibre reinforced soil bricks. *Constr. Build. Mater.* **2020**, *240*, 117806. [CrossRef]
24. Yang, S.; Song, Y.; Fang, H.; Wang, D.; Lu, W.; Huang, Y.; Zhao, C.; Chen, L.; Song, X. Fiber-reinforced microbially induced carbonate precipitation (MICP) for enhancing soil stability: Mechanisms, effects, and future prospects. *J. Build. Eng.* **2024**, *94*, 109955. [CrossRef]
25. Zhao, Y.; Yang, Y.; Ling, X.; Gong, W.; Li, G.; Su, L. Dynamic behavior of natural sand soils and fiber reinforced soils in heavy-haul railway embankment under multistage cyclic loading. *Transp. Geotech.* **2021**, *28*, 100507. [CrossRef]
26. Soltani, A.; Deng, A.; Taheri, A. Swell–compression characteristics of a fiber–reinforced expansive soil. *Geotext. Geomembr.* **2018**, *46*, 183–189. [CrossRef]
27. Yi, F.; Du, C. Triaxial Testing of Geosynthetics Reinforced Tailings with Different Reinforced Layers. *Materials* **2020**, *13*, 1943. [CrossRef] [PubMed]
28. Jia, P.; Khoshghalb, A.; Chen, C.; Zhao, W.; Dong, M.; Alipour Esgandani, G. Modified Duncan-Chang Constitutive Model for Modeling Supported Excavations in Granular Soils. *Int. J. Geomech.* **2020**, *20*, 04020211. [CrossRef]
29. Kumar, S.; Jat, M.K.; Sarkar, R.; Alsabhan, A.H. Static and dynamic characterization of fiber reinforced sand: A numerical investigation. *J. King Saud Univ.-Eng. Sci.* **2024**, *36*, 517–523. [CrossRef]
30. Bin, T.; Tianli, L.; Biaohe, Z. Duncan–Chang E-υ Model Considering the Thixotropy of Clay in the Zhanjiang Formation. *Sustainability* **2022**, *14*, 12258. [CrossRef]
31. Govindarajan, K.; Ramani, E.S. Effect of Nano Additive on Mechanical Properties of Natural Fiber Reinforced Soil. *J. Nat. Fibers* **2023**, *20*, 2143980. [CrossRef]
32. Shen, Y.S.; Tang, Y.; Yin, J.; Li, M.P.; Wen, T. An experimental investigation on strength characteristics of fiber-reinforced clayey soil treated with lime or cement. *Constr. Build. Mater.* **2021**, *294*, 123537. [CrossRef]
33. Lu, L.; Liu, C.; Qu, S.; Zhang, M. Experimental study on the mechanical and hydraulic behaviour of Fibre-Reinforced cemented soil with fly ash. *Constr. Build. Mater.* **2022**, *321*, 126374. [CrossRef]
34. Moslemi, A.; Tabarsa, A.; Mousavi, S.; Monfared, M.H.A. Shear strength and microstructure characteristics of soil reinforced with lignocellulosic fibers-Sustainable materials for construction. *Constr. Build. Mater.* **2022**, *356*, 129246. [CrossRef]
35. Song, Y.; Ding, J.; Yang, H.; Yang, W.; Xia, Y.; Zhu, T.; Lv, Z. Experimental study on dynamic elastic modulus and damping ratio of lignin-fiber-reinforced sandy soil. *Case Stud. Constr. Mater.* **2025**, *22*, e04592. [CrossRef]
36. *ASTM D2487-17*; Standard Practice for Classification of Soils for Engineering Purposes (Unified Soil Classification System). ASTM International: West Conshohocken, PA, USA, 2021.
37. Aldaood, A. Impact of fine materials on the saturated and unsaturated behavior of silty sand soil. *Ain Shams Eng. J.* **2020**, *11*, 717–725. [CrossRef]
38. Feia, S.; Sulem, J.; Canou, J.; Ghabezloo, S.; Clain, X. Changes in permeability of sand during triaxial loading: Effect of fine particles production. *Acta Geotech.* **2016**, *11*, 1–19. [CrossRef]
39. Ma, Q.; Xing, W.W.; Li, L.H.; Hu, X. Study on Flax Fiber-reinforced Sand by Triaxial Test. *J. Zhengzhou Univ. (Eng. Sci.)* **2018**, *39*, 56–60.
40. Jiang, X.; Guo, J.; Yang, H.; Bao, S.; Wen, C.; Chen, J. Study on Stress–Strain Relationship of Coir Fiber-Reinforced Red Clay Based on Duncan–Chang Model. *Appl. Sci.* **2022**, *13*, 556. [CrossRef]
41. Teng, Z.C.; Zhou, Y.D.; Teng, Y.C.; Liu, X.Y.; Liu, J.L.; Li, B. Deviatoric stress-strain curve construction with strain-softening account via the damage-modified Duncan-Chang, arctangent and informer models: A comparative analysis. *Front. Earth Sci.* **2023**, *11*, 1238286. [CrossRef]
42. Zeng, F.; Shao, L. Unloading elastic behavior of sand in cyclic triaxial tests. *Geotech. Test. J.* **2016**, *39*, 462–475. [CrossRef]